# Conformational and complexational study of some maleonitrile mixed oxadithia crown ethers by NMR spectroscopy and molecular modelling

**Erich Kleinpeter,*[a] Manuela Grotjahn,[a] Karel D. Klika,[b] Hans-Joachim Drexler[c] and Hans-Jürgen Holdt[c]**

[a] *Institut für Organische Chemie und Strukturanalytik, Universität Potsdam, D-14469, Potsdam, Germany*
[b] *Department of Chemistry, University of Turku, FIN-20014, Turku, Finland*
[c] *Institut für Anorganische Chemie und Didaktik der Chemie, Universität Potsdam, D-14469, Potsdam, Germany*

***Received (in Cambridge, UK) 24th November 2000, Accepted 6th April 2001***
***First published as an Advance Article on the web 1st May 2001***

The macrocyclic ring interconversion of four maleonitrile mixed oxadithia crown ethers of variable ring size, mn-12-$S_2O_2$, mn-15-$S_2O_3$, mn-18-$S_2O_4$ and fn-12-$S_2O_2$, were studied by $^1$H and $^{13}$C NMR spectroscopy and by molecular modelling. The barriers to ring interconversion were estimated using variable temperature NMR spectroscopy and from the calculated activation energies, together with the spin-lattice relaxation times of the $CH_2$ carbon atoms, conclusions were drawn regarding the intramolecular flexibility of the crown ethers in both the free state as well as the complexed state incorporating either $Ag^I$, $Bi^{III}$, $Sb^{III}$, $Pd^{II}$ or $Pt^{II}$ metal cations. Furthermore, both the stoichiometry of the complexes and the coordination sites of the crown ethers to the various cations were also clearly implicated. Molecular modelling was also utilised to ascertain the preferred conformers of the four compounds and their corresponding complexes, the results of which corroborated the experimental NMR results to a high degree.

## Introduction

The continuing interest in the oxygen-bearing crown ethers stems from their ability to selectively bind cations from complex solutions comprised of chemically similar cations. The preferred conformation for these oxa crown ethers is *endo*-dentate, in which the oxygen atoms are orientated towards the centre of the macrocyclic ring and the resultant cavity of negative electrostatic potential that this creates is selectively receptive towards cations of a particular diameter. The state of both the metal cation complexation and the attendant variation of the crown ether stereochemistry (and thereby more effective accommodation of the cations) can be readily assessed by NMR spectroscopy.[1] Furthermore, the stoichiometry of the complexes and their stability constants can also be readily determined by the application of NMR spectroscopy.[2]

Thia crown ethers, due to the longer C–S bond (1.8 Å) compared to the C–O bond (1.4 Å), prefer the *exo*-dentate conformation, *i.e.* the sulfurs are pointed away from the centre of the macrocyclic ring. As a result, the dihedral angle of the S–C–C–S segment in thia crowns is preferably *trans* (respectively *gauche* in the oxa crowns) and *gauche* for the C–C–S–C segment (respectively *trans* in the oxa crowns). Thus the differences in preference of the thia crowns in comparison to their oxygen-bearing analogues for complexation is accentuated relative to their single atom binding modes; whilst oxygen-bearing crown ethers tend to preferentially bind main group metal cations the corresponding thia crown ethers prefer transition metal cations.[3]

Recently, we synthesised a set of mixed oxadithia crown ethers [maleonitrile dithia crown ethers: mn-12-$S_2O_2$–mn-18-$S_2O_4$ and fn-12-$S_2O_2$ (**1**–**4**, see Scheme 1)] and determined that these mixed oxadithia crown ethers are highly receptive coronands which force *A*, *AB* and *B* class metal cations into their mixed S and O coordination spheres.[4–6] We report now the preferred conformations and the intramolecular flexibility of **1**–**4**, both in the free state and whilst complexed to a metal cation such as $Ag^I$, $Bi^{III}$, $Sb^{III}$, $Pd^{II}$ or $Pt^{II}$, which were found to readily coordinate to these mixed $S_2O_n$ coronands.[4–6]

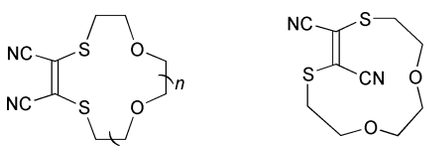


mn-12-$S_2O_2$ (*n*=1) **1**
mn-15-$S_2O_3$ (*n*=2) **2**
mn-18-$S_2O_4$ (*n*=3) **3**
fn-12-$S_2O_2$ **4**

**Scheme 1** Structures of the compounds studied.

## Results and discussion

### NMR studies

The assignment strategy of both the $^1$H and $^{13}$C NMR spectra of **1**–**4** was based on the assignment of the most upfield carbon signal as the aliphatic carbon bearing the sulfur, from which the rest of the assignments followed suit by the standard application of COSY, HMQC and HMBC experiments. The $^1$H signals for compounds **1**–**3** are all strongly exchange-broadened even at ambient temperature and, by way of example, the variable temperature $^1$H NMR spectra of mn-12-$S_2O_2$ (**1**) together with both the experimental and theoretical $^1$H NMR spectrum, simulated using the PERCH iterator program[7] of fn-12-$S_2O_2$ are presented in Fig. 1. The $^1$H chemical shifts for **1**–**3** are listed in Table 1; in Table 2 are listed the geminal and vicinal H–H coupling constants which could be extracted after

 DOI: 10.1039/b009453f

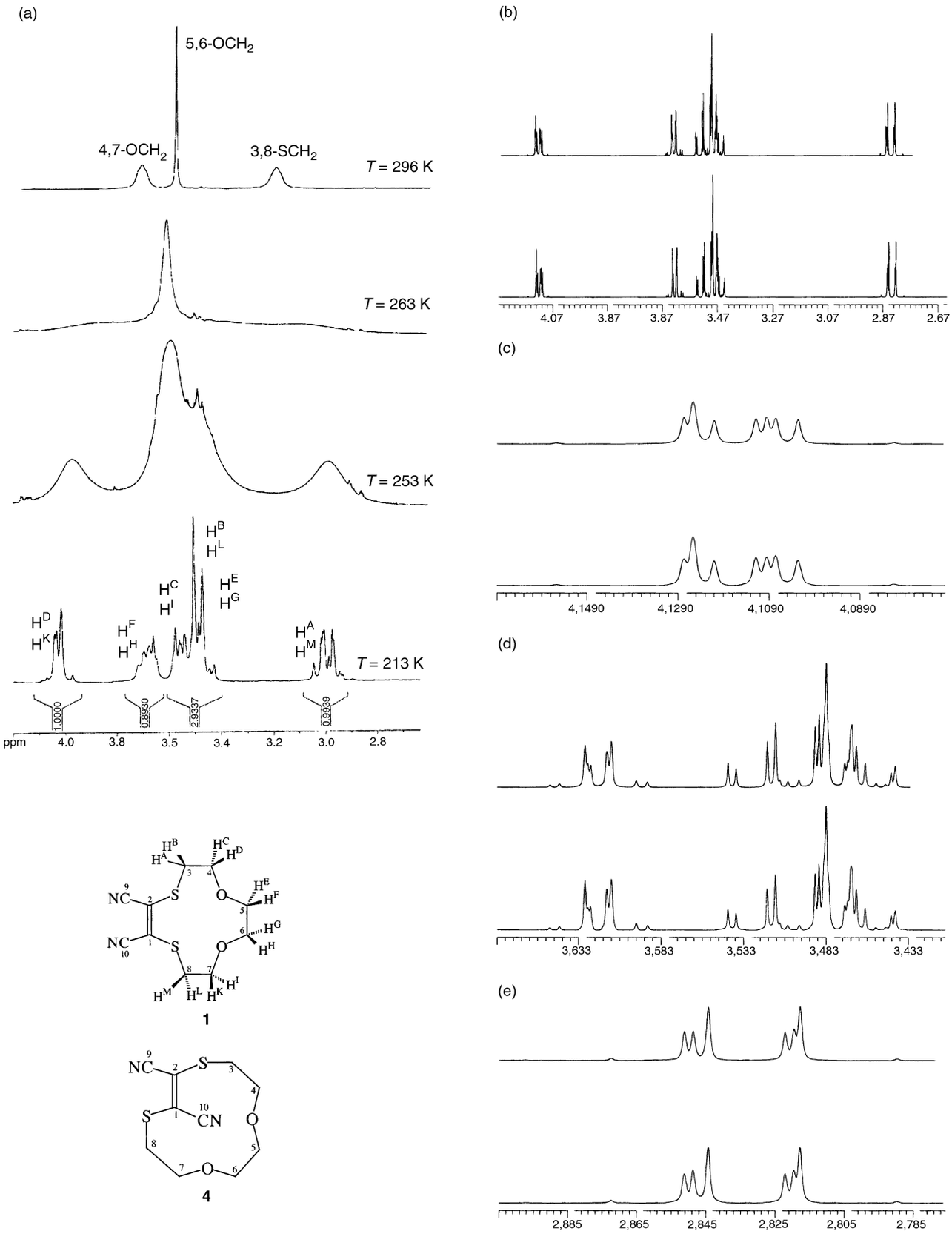


1

4

**Fig. 1** (a) $^1$H NMR spectra of mn-12-$S_2O_2$ (**1**) at various temperatures; (b) experimental (bottom) and theoretical (top) $^1$H NMR spectrum of fn-12-$S_2O_2$ (**4**) at ambient temperature, simulated using PERCH;[7] (c)–(e) expanded parts of (b).

simulation of the $^1$H NMR spectra for **1** at −55 °C and the $^1$H NMR spectra for **4** at 25 °C using PERCH (together with the $^1$H chemical shifts for **4**).[7] Compound **4** is a rigid structure and temperature variation did not result in any discernible dynamic effects. For compound **2**, a linewidth sufficiently small to enable extraction of the relevant coupling information after decoalescence could not be obtained; for compound **3**, decoalescence of the proton signals could not be accomplished at all. After calculation of the corresponding dihedral angles from the experimentally obtained vicinal H–H coupling constants, it is clear that *gauche* relationships are present for the framework atoms in both S–$CH_2$–$CH_2$–O structural fragments for the two compounds **1** and **4**. Similar conformational relationships for the structural fragments S–$CH_2$–$CH_2$–O to those obtained for **1**

**Table 1** $^1$H chemical shifts in ppm relative to TMS for compounds mn-12-$S_2O_2$–mn-18-$S_2O_4$ (**1**–**3**) and their $Ag^I$, $Bi^{III}$, $Sb^{III}$, $Pd^{II}$ or $Pt^{II}$ complexes ($\Delta\delta$) in $NO_2CD_3$ at 25 °C

| Compound | $SCH_2CH_2O$ | $SCH_2CH_2O$ | $OCH_2CH_2O$ |
|---|---|---|---|
| mn-12-$S_2O_2$ (**1**) | 3.25 | 3.75 | 3.60 |
| [Ag(mn-12-$S_2O_2$)$_2$]$PF_6$ | +0.31 | +0.02 | +0.24 |
| [Ag(mn-12-$S_2O_2$)$_2$]$ClO_4$ | +0.29 | +0.01 | +0.22 |
| [Pd(mn-12-$S_2O_2$)$_2$]$Cl_2$ | 3.73–3.77; 3.80–3.82 | 3.86–3.88; 3.90–3.91 | 4.11–4.13; 4.14–4.16 |
| [Pt(mn-12-$S_2O_2$)$_2$]$Cl_2$ | 3.84–3.86; 3.87–3.88 | 3.75–3.82; 3.84–3.86 | 3.87–3.88; 4.20–4.28 |
| mn-15-$S_2O_3$ (**2**) | 3.38 | 3.72 | 3.58 |
| [Ag(mn-15-$S_2O_3$)$_2$]$PF_6$ | +0.16 | +0.05 | +0.12 |
| [Ag(mn-15-$S_2O_3$)]$ClO_4$ | +0.31 | +0.10 | +0.23 |
| [Bi(mn-15-$S_2O_3$)]$Cl_3$ | +0.06 | +0.11 | +0.09 |
| [Sb(mn-15-$S_2O_3$)]$Cl_3$ | +0.02 | +0.03 | +0.05 |
| mn-18-$S_2O_4$ (**3**) | 3.38 | 3.76 | 3.62 |
| [Ag(mn-18-$S_2O_4$)]$PF_6$ | +0.20 | +0.01 | +0.20 |
| [Bi(mn-18-$S_2O_4$)]$Cl_3$ | +0.07 | +0.39 | +0.29 |
| [Sb(mn-18-$S_2O_4$)]$Cl_3$ | +0.05 | +0.14 | +0.12 |
| [Pd(mn-18-$S_2O_4$)]$Cl_2$ | 3.67–3.83; broad, m | 3.60; s | 3.67–3.83; broad, m |
| [Pt(mn-18-$S_2O_4$)]$Cl_2$ | 3.62–3.72, broad, m | 3.59; s | 3.62–3.72; broad, m |

**Table 2** $^1$H chemical shifts in ppm relative to TMS for mn-12-$S_2O_2$ (**1**) (at −55 °C) and fn-12-$S_2O_2$ (**4**) (at 25 °C) both in $CD_2Cl_2$ at 500 MHz together with their geminal and vicinal $^1$H–$^1$H coupling constants in Hz extracted by PERCH iteration[7]

| Compound | $-SCH_AH_BCH_CH_DO-$ | | | | $-OCH_EH_FCH_{E'}H_FO-$ | |
|---|---|---|---|---|---|---|
| | $H_A$ | $H_B$ | $H_C$ | $H_D$ | $H_E$ | $H_F$ |
| mn-12-$S_2O_2$ (**1**) | 3.48 | 2.99 | 3.49 | 4.02 | 3.55 | 3.62 |
| fn-12-$S_2O_2$ (**4**) | 3.51 | 2.83 | 3.47 | 4.12 | 3.48 | 3.62 |
| | $J_{A,B}$ | $J_{A,C}$ | $J_{A,D}$ | $J_{B,C}$ | $J_{B,D}$ | $J_{C,D}$ |
| mn-12-$S_2O_2$ (**1**) | −15.3 | 12.0 | 3.2 | 2.3 | 2.1 | −9.8 |
| fn-12-$S_2O_2$ (**4**) | −15.2 | 11.9 | 2.9 | 2.0 | 2.2 | −9.6 |
| | $J_{E,F}$ | $J_{E,E'}$ | $J_{E,F'}$ | $J_{F,F'}$ | | |
| mn-12-$S_2O_2$ (**1**) | −11.9 | 6.3 | 2.0 | 0.8 | | |
| fn-12-$S_2O_2$ (**4**) | −10.0 | 10.7 | 1.9 | 1.8 | | |

and **4** however, can also be inferred for the larger heterocyclic ring systems **2** and **3**. The electronegative effect of the oxygen atoms, with respect to the sulfur atoms, can also be seen in the coupling constants of these crown ether moieties: $J_{A,D}$ 2.9 and 3.2 Hz > $J_{B,C}$ 2.0 and 2.3 Hz, respectively.

In Table 3 are listed the $^{13}$C chemical shifts for **1**–**4** from which it is seen that the $^{13}$C NMR shifts of the two (*Z*) and (*E*) isomers, **1** and **4**, bear a strong resemblance to one another. Tables 1 and 3 also list the $^1$H and $^{13}$C chemical shifts, respectively, of the crown ethers when complexed to $Ag^I$, $Bi^{III}$, $Sb^{III}$, $Pd^{II}$ or $Pt^{II}$ cations. From these data, pertinent observations regarding the relative strength, position and stoichiometry of the complexation can be drawn. Firstly, because of the similar $^{13}$C chemical shift variations for all of the analogous carbons of **1**–**3** on complexation to $Ag^I$, it can be inferred that there is equal coordination of the $Ag^I$ cation to all of the macrocyclic ring heteroatoms with the anion having only a negligible influence on the chemical shifts. Titration curves indicate a 1 : 1 complexation for **1** to $Ag^I$ but, by way of deviation, they indicate the formation of a 2 : 3 complex for **2**[9] to the same cation—in agreement with the X-ray structure determination of the material in the solid state.[10] Since the $^{13}$C chemical shift variations are largest for **1**, it can be concluded that the complexation of the $Ag^I$ cation to **1** is stronger than to either **2** or **3**.

Secondly, conspicuous for $Bi^{III}$ and $Sb^{III}$ complexation is the higher field shift of the $OCH_2$ protons and corresponding carbon atoms compared to the $SCH_2$ chemical shift variations in **1**–**3** and hence the preferred complexation of both the $Bi^{III}$ and $Sb^{III}$ cations in these ether complexes is to the oxygen atoms over the sulfur atoms. These chemical shift variations are significantly larger in the $BiCl_3$ complexes and imply that these complexes are more stable in comparison to the $Sb^{III}$ complexes for the same sized ring.

Finally, contrastingly for the complexation of $Pd^{II}$ and $Pt^{II}$ to **1**–**3**, the $SCH_2$ protons and carbons, together with the carbon atoms of the maleonitrile moiety, are strongly shifted to lower field; the $OCH_2$ protons and carbons of the crown moiety, however, are only negligibly affected. As determined in the solid state,[10] and hence also in solution, the two cations $Pd^{II}$ and $Pt^{II}$ are complexed in an *exo*-cyclic mode to the sulfur atoms only. The stoichiometry of the corresponding complexes was shown to be 1 : 1[11] and the $PtCl_2$ complexes are also more stable than their $PdCl_2$ analogues. In comparison of three crown ethers, **1**–**3**, the following stability order was established based on the strength of the chemical shift variations during the titration experiments.

[M(mn-12-$S_2O_2$)]$Cl_2$ > [M(mn-18-$S_2O_4$)]$Cl_2$ > [M(mn-15-$S_2O_3$)]$Cl_2$

These results are in agreement with previous UV–VIS results[4] and a parallel mass spectrometry study.[12]

## Dynamic NMR studies

The exchange-broadened resonances of both **1** and **2** are fully resolved at lower temperature (see Fig. 1) enabling the ready determination of the coalescence temperatures and estimation of the corresponding ring interconversion barriers (activation free energies) *via* the Eyring equation.[8] The barriers to ring interconversion are presented in Table 4. The corresponding values could not be accurately determined for **3**, even at the lowest temperature attainable with the available NMR set-up, for the signals still remained considerably exchange-broadened even at the extreme limit [−120 °C ($CD_2Cl_2$–$CCl_2FH$, 10 : 90) at 300 MHz]. Therefore, a barrier to interconversion for **3** of $\Delta G^{\ddagger} < 25$ kJ mol$^{-1}$ could only be estimated. In addition to the free crown ethers, the $Ag^I$ and $Bi^{III}$ complexes of **1** and **2** were also examined and evaluated by dynamic NMR, the results of which are also included in Table 4.

The following two conclusions regarding the intramolecular flexibility of **1**–**3** and their respective $Ag^I$ and $Bi^{III}$ complexes could be drawn from the barriers to ring interconversion. Firstly, the macrocyclic ring interconversion barrier decreases as the ring size increases [**1** (~52 kJ mol$^{-1}$) > **2** (~33 kJ mol$^{-1}$) > **3** (<25 kJ mol$^{-1}$)]; *i.e.* the intramolecular flexibility increases significantly, probably *via* a pseudo-rotational mode. Secondly, the complexation of either $Ag^I$ or $Bi^{III}$ cation to **2** increases the barrier to ring interconversion of the corre-

**Table 3** $^{13}C$ chemical shifts in ppm relative to TMS for compounds mn-12-$S_2O_2$–mn-18-$S_2O_4$, fn-12-$S_2O_2$ (**1**–**4**) and their $Ag^I$, $Bi^{III}$, $Sb^{III}$, $Pd^{II}$ or $Pt^{II}$ complexes (in $\Delta\delta$) in $NO_2CD_3$ at 25 °C

| Compound | *C*=C | S*C*$H_2$O | SC$H_2$*C*$H_2$O | O*C*$H_2$C$H_2$O | *C*≡N |
|---|---|---|---|---|---|
| mn-12-$S_2O_2$ (**1**) | 127.19 | 37.16 | 71.46 | 69.67 | 115.43 |
| [Ag(mn-12-$S_2O_2$)$_2$]$PF_6$ | −0.84 | +0.25 | −5.21 | −0.70 | −1.69 |
| [Ag(mn-12-$S_2O_2$)$_2$]$ClO_4$ | −0.79 | +0.27 | −4.89 | −0.76 | −1.59 |
| [Pd(mn-12-$S_2O_2$)$_2$]$Cl_2$ | +3.39 | +5.82 | −3.13 | −0.19 | −4.07 |
| [Pt(mn-12-$S_2O_2$)$_2$]$Cl_2$ | +4.15 | +6.44 | −3.11 | −0.80 | −4.15 |
| mn-15-$S_2O_3$ (**2**) | 123.58 | 36.28 | 70.84 | 71.19; 71.65 | 114.49 |
| [Ag(mn-15-$S_2O_3$)$_2$]$PF_6$ | +0.02 | +0.94 | −1.71 | −0.16; −0.43 | −0.81 |
| [Ag(mn-15-$S_2O_3$)]$ClO_4$ | +0.09 | +1.80 | −3.33 | −0.40; −0.69 | −1.57 |
| [Bi(mn-15-$S_2O_3$)]$Cl_3$ | +0.26 | +0.06 | −0.52 | −0.49; −0.31 | −0.43 |
| [Sb(mn-15-$S_2O_3$)]$Cl_3$ | +0.21 | +0.04 | −0.36 | −0.30; −0.20 | −0.19 |
| [Pd(mn-15-$S_2O_3$)]$Cl_2$ | — | +8.80 | +0.14 | -0.24; −0.75 | — |
| [Pt(mn-15-$S_2O_3$)]$Cl_2$ | — | +9.20 | +0.34 | -0.14; −0.50 | −2.68 |
| mn-18-$S_2O_4$ (**3**) | 123.30 | 36.37 | 70.36 | 71.62; 71.81; 71.91 | 114.18 |
| [Ag(mn-18-$S_2O_4$)]$PF_6$ | 0.28 | +0.57 | −1.86 | −1.14; −0.77; −0.44 | −0.72 |
| [Bi(mn-18-$S_2O_4$)]$Cl_3$ | +1.37 | −1.48 | −0.72 | −1.84; −1.22; −1.12 | −0.01 |
| [Sb(mn-18-$S_2O_4$)]$Cl_3$ | +0.35 | −0.43 | −0.08 | −0.91; −0.91; −0.75 | −0.02 |
| [Pd(mn-18-$S_2O_4$)]$Cl_2$ | — | +8.45 | −2.31 | -0.11; —; — | — |
| [Pt(mn-18-$S_2O_4$)]$Cl_2$ | — | +8.40 | −2.30 | -0.21; —; — | — |
| fn-12-$S_2O_2$ (**4**) | 125.58 | 36.34 | 73.63 | 71.88 | 114.98 |

**Table 4** Coalescence temperatures, $T_C$, in K and activation free energies, $\Delta G_C^{\ddagger}$ in kJ $mol^{-1}$ for compounds **1** and **2** together with some of their $Ag^I$ and $Bi^{III}$ complexes

| Compound | Solvent | S*C*$H_2$CH$_2$O $T_C$, $\Delta G_C^{\ddagger}$ | SCH$_2$*C*$H_2$O $T_C$, $\Delta G_C^{\ddagger}$ | O*C*$H_2$CH$_2$O $T_C$, $\Delta G_C^{\ddagger}$ |
|---|---|---|---|---|
| mn-12-$S_2O_2$ (**1**) | $CD_2Cl_2$ | 263, 51.5 | 263, 51.7 | 253, 51.4 |
| [Ag(mn-12-$S_2O_2$)$_2$]$ClO_4$ | $CD_2Cl_2$ | 253, 51.9 | 258, 51.7 | — |
| [Ag(mn-12-$S_2O_2$)$_2$]$PF_6$ | $CD_2Cl_2$ | 248, 50.6 | 258, 50.0 | — |
| mn-15-$S_2O_2$ (**2**) | $CD_2Cl_2$–$CCl_2FH$ | 173, 32.7 | 173, 33.6 | — |
| [Ag(mn-15-$S_2O_3$)]$ClO_4$ | $(CD_3)_2CO$ | — | 198, 37.0 | — |
| [Ag(mn-15-$S_2O_3$)$_2$]$PF_6$ | $(CD_3)_2CO$ | — | 188, 37.0 | — |
| [Bi(mn-15-$S_2O_3$)]$Cl_3$ | $(CD_3)_2CO$ | 193, 37.9 | 188, 36.1 | — |

**Table 5** $^{13}C$ spin-lattice relaxation times, $T_1$, in seconds for the aliphatic carbons of compounds **1**–**3** together with some of their $Ag^I$ and $Bi^{III}$ complexes in $CD_3NO_2$

| Compound | –S*C*$H_2$– | –*C*$H_2$O– | –*C*$H_2$– | –*C*$H_2$O– | –*C*$H_2$– |
|---|---|---|---|---|---|
| mn-12-$S_2O_2$ (**1**) | 1.46 | 1.64 | 163 | — | — |
| [Ag(mn-12-$S_2O_2$)$_2$]$ClO_4$ | 0.46 | 0.69 | 0.58 | — | — |
| mn-15-$S_2O_3$ (**2**) | 1.13 | 1.22 | 1.34 | 1.29 | — |
| [Ag(mn-15-$S_2O_3$)]$ClO_4$ | 0.59 | 0.67 | 0.62 | 0.63 | — |
| [Bi(mn-15-$S_2O_3$)]$Cl_3$ | 0.81 | 0.90 | 1.09 | 0.94 | — |
| mn-18-$S_2O_4$ (**3**) | 0.91 | 1.16 | 1.25 | 1.48 | 1.25 |
| [Bi(mn-18-$S_2O_4$)]$Cl_3$ | 0.67 | 0.65 | 0.79 | 0.78 | 0.76 |

sponding crown ether. Evidently complexation forces the crown ether moiety into a particular conformation to accommodate the cation thereby reducing the intramolecular flexibility of the macrocyclic ring. By contrast, the barrier to ring interconversion of **1** was essentially invariant upon complexation ($\Delta G^{\ddagger}$ *ca.* 50–52 kJ $mol^{-1}$). The anion again appeared to have only a negligible effect, *cf.* the $AgClO_4$ and $AgPF_6$ complexes.

### Longitudinal relaxation NMR studies

The utilisation of dynamic NMR is limited to cases where one is able to freely access the coalescence temperature and lower temperatures. In order to obtain some indication of the intramolecular flexibility of **3** and its $Bi^{III}$ complex, as well as to substantiate the dynamic NMR results obtained above for **1** and **2** and their complexes, the spin-lattice relaxation time ($T_1$) of the aliphatic carbons of **1**–**3** together with some of their $Ag^I$ and $Bi^{III}$ complexes were measured using the inversion–recovery pulse sequence. $T_1$ values reflect both the inter- and intramolecular motion (and therein flexibility) of the nuclei under measurement. In the case of molecules tumbling isotropically in solution, implicit information regarding the intramolecular flexibility is readily available from eqn. (1),[13] where $1/T_{1\text{-DD}}$ is

$$1/T_{1\text{-DD}} = Nh^2\gamma_C^2\gamma_H^2\tau_C r_{CH}^{-6} \quad (1)$$

the dipole–dipole relaxation, $N$ the number of Hs, $r_{CH}$ the internuclear distance and $\tau_C$ the molecular correlation time.

The portion of the spin-lattice relaxation time, $T_1$, which is due to the dipole–dipole relaxation, $T_{1\text{-DD}}$, can be readily estimated from the experimentally measured $T_1$ by measurement of the NOE enhancement factor $\eta$ and eqn. (2).

$$T_{1\text{-DD}} = T_1(1.988/\eta) \quad (2)$$

For compounds **1**–**3** and their $Ag^I$ and $Bi^{III}$ complexes, NOE enhancements of 82–93% ($\eta = 0.82$–$0.93$) were measured and together with the experimentally-determined $T_1$ values (see Table 5), were used as a basis for the following qualitative conclusions regarding the intramolecular flexibility of **1**–**3** and their $Ag^I$ and $Bi^{III}$ complexes. Firstly, increasing ring size reduces $T_1$ as the larger the ring, the slower its reorientation, reducing $T_1$ substantially. This correlation has been found previously for the cycloalkanes.[14] Thus there are two opposing factors—intermolecular and intramolecular motion—with the

increase in the ring size tending to reduce the $T_1$ values by the reduced motion of the molecule as a whole being countered by the additional flexibility within the molecule leading to an increase in $T_1$. With these macrocycles, the reduction in the $T_1$ values afforded by the increased ring size more than compensates for the increase in $T_1$ factored in by the additional flexibility of the ring—which has already been established from the dynamic NMR experiments. Thus, only within a series of the same ring size can decisive conclusions be drawn regarding molecular flexibility and measured $T_1$ values.

As an unwavering trend, though, the $T_1$ values of the $SCH_2$ carbon atoms near the rigid maleonitrile moiety are slightly shorter in comparison to the $OCH_2$ carbons for this very reason of reduced local intramolecular motion. Complexation, however, clearly reduces the $T_1$ values of the carbon atoms involved in the crown ether moiety, as expected, and concluded from the aforementioned dynamic NMR results. This reduction in the $T_1$ values is a consequence of the restricted flexibility as a direct result of the formation of the complexes. Notably, $T_1$ values of all the carbon atoms of the crown ether moiety are similarly reduced in the $Ag^I$ complexes of mn-12-$S_2O_2$–mn-18-$S_2O_4$ (**1**–**3**) corroborating the conclusion based on the chemical shift variations regarding the full (*i.e.* equal) complexation of the $Ag^I$ cation to all hetero donor atoms of the crown ether. Finally, complexation to $Bi^{III}$ also reduces the intramolecular flexibility of the crown ether moiety; in the case of mn-18-$S_2O_4$ (**3**), however, the $T_1$ values of the $OCH_2$ carbons are reduced more distinctly than the $SCH_2$ carbons within the same molecule. As concluded previously from the chemical shift variations, the reason is the preferred complexation of the $Bi^{III}$ cation to the oxygen atoms over the sulfur atoms.

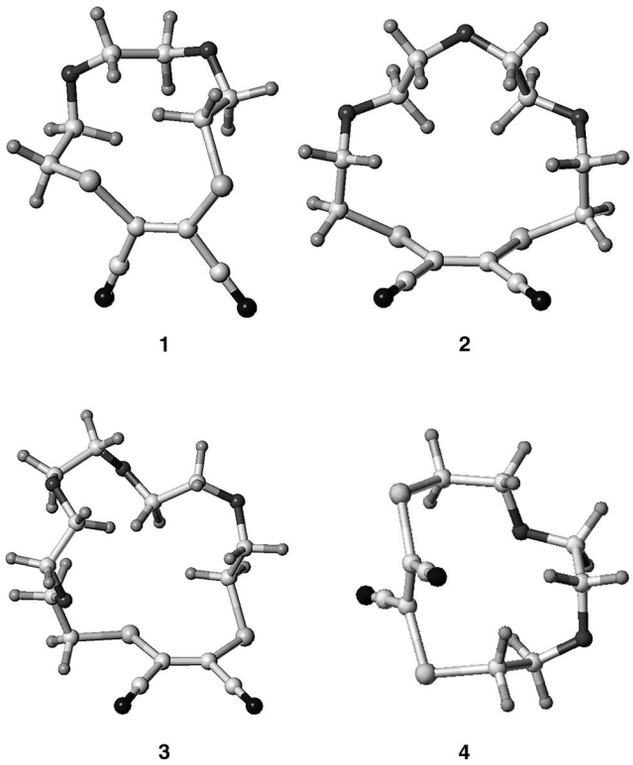


**Fig. 2** Global minimum structures of mn-12-$S_2O_2$–mn-18-$S_2O_4$ (**1**–**3**) and fn-12-$S_2O_2$ (**4**).

### Molecular modelling studies

Since the only specific information on the preferred conformers of mn-12-$S_2O_2$–mn-18-$S_2O_4$ (**1**–**3**) was obtained from the $^1H$ NMR spectra of frozen mn-12-$S_2O_2$ (**1**) and fn-12-$S_2O_2$ (**4**), and because only *gauche* conformations for the $–SCH_2CH_2O–$ crown ether fragments in **1** and **4** could be deduced, a molecular modelling study was also conducted in order to determine the complete preferred conformations of the crown ethers **1**–**3**. In addition to molecular dynamic simulations at 500 K, GRIDSEARCH calculations, carefully varying all dihedral angles in 10° steps, were also processed starting from known X-ray structures. The conformations of minimal energy, thus obtained, were geometry optimised first by the TRIPOS force field (for the complexes the MSI/DISCOVER 97 force field[15]) and afterwards by PM3 semi-empirical quantum-chemical calculations. As a final result, usually a number of conformations of similar energies were obtained of which the most stable one for mn-12-$S_2O_2$–mn-18-$S_2O_4$ is depicted in Fig. 2. The following trend is visible: C–C–S–C fragments prefer *gauche*, S–C–C–O *anti* and O–C–C–O fragments both *gauche* and *anti* conformations in agreement with expectations.[16] The maleonitrile fragment remains rigid and the angle of the aliphatic arms to this plane, NC–C–S–$CH_2$, was dependent on the size of the macrocyclic ring system.

The calculation results obtained for the complexes are quite compelling—the "sandwich-like" coordination of $Ag^I$ employing all ring hetero donor atoms of compounds **1**–**3**[9] and the *exo*-dentate orientation of the $Pd^{II}$ and $Pt^{II}$ cations to compounds **1**–**3**,[11] both in complete agreement with the experimental results of this study, were correctly predicted and have been published previously. However, the experimental results obtained for the $Bi^{III}$ and $Sb^{III}$ complexes are impressively corroborated by the molecular modelling performed in this study. The two cations coordinate in a "half-sandwich-like" conformation to compounds **1**–**3** and the global minimum structures of both [Bi(mn-15-$S_2O_3$)]$Cl_3$ and [Sb(mn-15-$S_2O_3$)]$Cl_3$ are depicted in Fig. 3. In the $Bi^{III}$ and $Sb^{III}$ complexes of

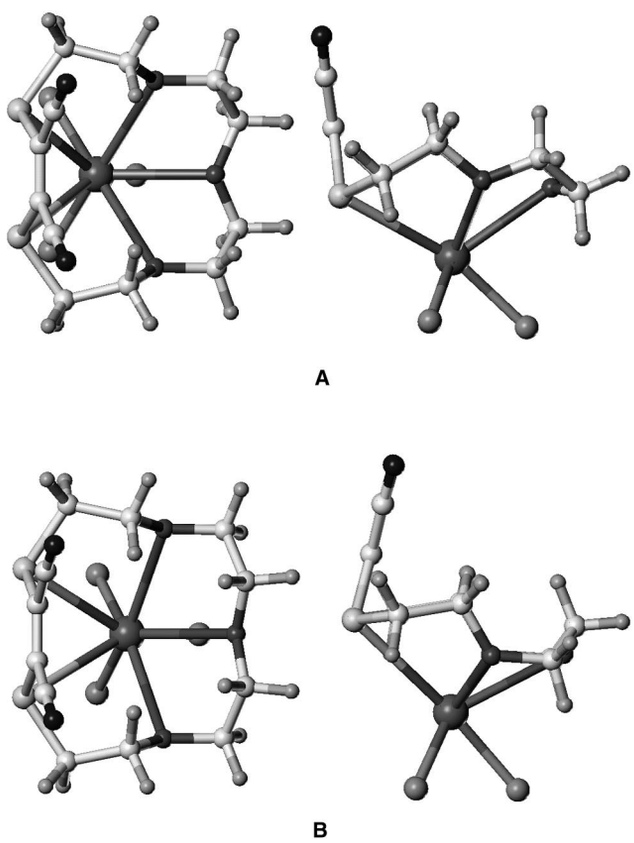


**Fig. 3** Global minimum structures of [Bi(mn-15-$S_2O_3$)]$Cl_3$ (**A**) and [Sb(mn-15-$S_2O_3$)]$Cl_3$ (**B**).

**1** and **2** and in the $Sb^{III}$ complex of **3**, the two cations coordinate to the two sulfur atoms and all the oxygen atoms of the crown ether moiety; in the $Bi^{III}$ complex of **3**, however, the sulfur atoms are not involved in the complexation of the crown ether moiety to the $Bi^{III}$ cation, this poignant result also distinctly corroborates the experimental NMR results.

## Conclusions

Both global minimum structures and the intramolecular flexibility of a number of mixed S, O coronands, compounds **1**–**3**, and their associated complexes formed with $Ag^{I}$, $Bi^{III}$, $Sb^{III}$, $Pd^{II}$ or $Pt^{II}$ metal cations were studied by NMR (including variable temperature NMR and $T_1$ spin-lattice relaxation time measurements) and by molecular modelling. Complexation was found to clearly reduce the intramolecular flexibility. While $Ag^{I}$ coordinates more or less equivalently to all sulfur and oxygen donor atoms, $Bi^{III}$ and $Sb^{III}$ cations prefer the oxygen atoms of the crown ether moiety. By contrast, $Pt^{II}$ and $Pd^{II}$ coordinate in an *exo*-cyclic mode to the sulfur atoms only. Global minimum structures of compounds **1**–**3** and their respective $Ag^{I}$, $Bi^{III}$, $Sb^{III}$, $Pd^{II}$ and $Pt^{II}$ complexes were derived by molecular modelling and the results were found to be in excellent agreement with the experimentally obtained results.

## Experimental

### NMR spectroscopy

$^{1}H$ and $^{13}C$ NMR spectra were acquired on a Bruker ARX 300 NMR spectrometer equipped with a 5 mm probe operating at 300.13 and 74.47 MHz, respectively. All samples were dissolved in $CD_3NO_2$ or, in the case of low-temperature measurements, in $CD_2Cl_2$, $d_6$-acetone or in the mixed solvent system $CD_2Cl_2$–$CCl_2FH$ (10 : 90). Both $^{1}H$ and $^{13}C$ spectra were acquired using 30° pulses, 2 s relaxation delay, 32 K data points and referenced to TMS (0 ppm). For COSY, HMQC, and HMBC experiments the standard Bruker software was employed. Sample preparation consisted of five freeze–thaw cycles followed by sealing under argon.

For dynamic NMR measurements, the chemical shift differences, $\Delta\nu$/Hz, at the coalescence temperature, $T_C$, were determined by extrapolation from regions of slow exchange and the ring interconversional barriers $\Delta G^{\ddagger}$ were calculated in the usual way from these two values.[8] The probe temperature was calibrated using methanol to within ±1–2 °C.

The $T_1$ values were obtained using the inversion–recovery pulse sequence (12 delays) and evaluated using standard BRUKER software (errors for determining both the $T_1$ values and the NOE enhancement factors are 5–10%). NOEs were quantitatively determined from $^{13}C$ NMR spectra acquired with inverse-gated decoupling and determining the ratio of the integrals to BB-decoupled $^{13}C$ NMR spectra to estimate the NOE enhancement $\eta_{CH}$ and hence the contribution of $T_{1\text{-DD}}$ to $T_1$.[13]

### Molecular modelling

The molecular dynamic simulations (NVT statistical ensemble) of the crown ethers and their complexes were performed using the program MSI/DISCOVER97[15] (ESFF force field).[17] The ESFF has been shown to reproduce the structures of metal complexes with high accuracy and it is able to deal with a broad variety of metal centres without extensive reparametrisation.[18] The non-bonded interactions (long-range Coulomb and van der Waals forces) were calculated pairwise without cut-off. Energy minimisations were performed until the absolute value of the largest partial derivatives of the energy with respect to the coordinates was below 0.001 kcal $mol^{-1}$ $Å^{-1}$. Steepest descent and conjugated gradient (Polak–Ribiere scheme) methods, the quasi-Newton–Raphson algorithm in combination with the BFGS update scheme were used.[19] The MD runs were executed with time steps of 1 fs. Each MD run was carried out up to 510 ps at different temperatures ($T$ = 300, 373, 500 K) in order to explore the conformational space efficiently. During the first 10 ps the system was equilibrated. For data sampling the coordinates were saved every ps. After the MD simulation each of the saved structures was used as starting geometry for a subsequent ESFF energy minimisation.

The flexibility of the ligands (energy hypersurface) was also studied by the Grid search algorithm of SYBYL[20] (TRIPOS force field).[21] A step width of 10° about all rotatory bonds (OCCO, SCCO) was used. For non bonded interactions, described by van der Waals forces and long-range Coulomb interactions, an atom-based cut-off at 8 Å was imposed. Atomic charges were evaluated by the Gasteiger Marsili scheme.[22]

The heats of formation were calculated semi-empirically using the PM3[23] computational method within the MOPAC[24] program. All calculations were performed on either a Silicon Graphics IRIS-INDIGO XS24 or an IBM RS6000 machine.


## Acknowledgements

The kind help of Professor Reino Laatikainen and Dipl.-Chem. Matthias Niemitz (University of Kuopio, Finland), Dr Matthias Heydenreich, Dipl.-Chem. Gunther Wolf and Dipl.- Chem. Anja Holzberger (Universität Potsdam) and Dr Dieter Ströhl (Martin-Luther-Universität Halle-Wittenberg) is gratefully acknowledged.


## References


1 F. Vögtle and E. Weber, *Crown Ethers and Analogues*, Eds. S. Patai and Z. Rappoport, Wiley & Sons, New York, 1989; L. F. Lindoy, *The Chemistry of Macrocyclic Ligand Complexes*, Cambridge University Press, Cambridge, 1989; R. M. Izatt, K. Pawlak, J. S. Bradshaw and R. L. Bruening, *Chem. Rev.*, 1991, **91**, 1721; E. Kleinpeter, *J. Prakt. Chem.*, 1991, **333**, 817.
2 R. M. Izatt and J. J. Christensen, *Synthesis of Macrocycles. The Design of Selective Complexing Agents*, Wiley-Interscience, New York, 1987; D. J. Cram, *J. Inclusion Phenom.*, 1988, **6**, 397; J. M. Lehn, *J. Inclusion Phenom.*, 1988, **6**, 351; A. V. Bajaj and N. S. Poonia, *Coord. Chem. Rev.*, 1988, **87**, 55; S. Stoss, W. Schroth and E. Kleinpeter, *Magn. Reson. Chem.*, 1992, **30**, 425.
3 M. Hiraoka, *Studies in Organic Chemistry 12: Crown Compounds*, Elsevier, Amsterdam, 1982.
4 H.-J. Holdt, *Pure Appl. Chem.*, 1993, **65**, 477.
5 H.-J. Drexler, H. Reinke and H.-J. Holdt, *Z. Anorg. Allg. Chem.*, 1998, **624**, 1376.
6 H.-J. Drexler, I. Starke, M. Grotjahn, H. Reinke, H.-J. Holdt and E. Kleinpeter, *Z. Naturforsch., Teil B*, 1999, **54**, 799.
7 R. J. Laatikainen, *Magn. Reson.*, 1991, **92**, 1; R. Laatikainen, *QCPE Bull.*, 1992, **12**, 23; R. Laatikainen, M. Niemitz, U. Weber, J. Sundelin, T. Hassinen and J. Vepsäläinen, *J. Magn. Reson.*, 1996, **A120**, 1.
8 J. Sandström, *Dynamic NMR Spectroscopy*, Academic Press, London, 1982.
9 M. Grotjahn, H.-J. Drexler, N. Jäger, H.-J. Holdt and E. Kleinpeter, *J. Mol. Model.*, 1997, **3**, 355.
10 H.-J. Drexler, H. Reinke and H.-J. Holdt, *Chem. Ber.*, 1996, **129**, 807.
11 M. Grotjahn, H.-J. Drexler, N. Jäger, H.-J. Holdt and E. Kleinpeter, *J. Mol. Model.*, 1999, **5**, 72.
12 I. Starke, M. Grotjahn, H.-J. Drexler, H.-J. Holdt and E. Kleinpeter, *Inorg. Chim. Acta*, 2001, **317**, 133.
13 K. Pihlaja and E. Kleinpeter, *Carbon-13 NMR Chemical Shifts in Structural and Stereochemical Analysis*, VCH, New York, 1994, p. 349–352.
14 S. Berger, F. R. Kreissl and J. D. Roberts, *J. Am. Chem. Soc.*, 1974, **96**, 4348.
15 DISCOVER 2.9.7 & 95.0/3.00 User Guide, October 1995, San Diego, Biosym/MSI, 1995.
16 S. E. Hill and D. Feller, *J. Phys. Chem.*, 2000, **104**, 652.
17 S. Barlow, A. L. Rohl, S. Shi, C. H. Freeman and D. O'Hare, *J. Am. Chem. Soc.*, 1996, **118**, 7578.
18 N. Jäger and U. Schilde, *Struct. Chem.*, 1998, **9**, 77.
19 (*a*) R. Fletcher, *Practical Methods of Optimization*, Wiley & Sons, London, 1980; (*b*) R. Fletcher and M. J. D. Powell, *Comput. Chem.*, 1963, **6**, 163.
20 SYBYL 6.3, Tripos Assoc., St. Louis, MO, USA, 1996.
21 M. Clark, R. D. Cramer III and N. Van Opdenbosch, *J. Comput. Chem.*, 1989, **10**, 982.
22 J. Gasteiger and M. Marsili, *Org. Magn. Reson.*, 1981, **15**, 353.
23 J. J. P. Stewart, *J. Comput. Chem.*, 1989, **10**, 209.
24 J. J. P. Stewart, MOPAC 6.0, QCPE No. 455.